

# Detecting Optic Disk Based on AdaBoost and Active Geometric Shape Model

Zhun Fan

Guangdong Provincial Key Laboratory of Digital Signal and Image Processing, School of Engineering, Shantou University, Guangdong, China.  
Email:zfan@stu.edu.cn

Yibiao Rong

Guangdong Provincial Key Laboratory of Digital Signal and Image Processing, School of Engineering, Shantou University, Guangdong, China.  
Email:13ybrong@stu.edu.cn

Xinye Cai

School of Computer Science and Technology, Nanjing University of Aeronautics and Astronautics, Jiangsu, China  
Email:xinye@nuaa.edu.cn

Fang Li

Guangdong Provincial Key Laboratory of Digital Signal and Image Processing, School of Engineering, Shantou University, Guangdong, China.  
Email:13fli@stu.edu.cn

Wenji Li

Guangdong Provincial Key Laboratory of Digital Signal and Image Processing, School of Engineering, Shantou University, Guangdong, China.  
Email:wenji\_li@126.com

Huibiao Lin

Guangdong Provincial Key Laboratory of Digital Signal and Image Processing, School of Engineering, Shantou University, Guangdong, China.  
Email:13hblin@stu.edu.cn

**Abstract**— Detecting the optic disk (OD) is very important in the fundus image analysis. In this paper, we propose a new OD detection algorithm consisting of four main steps: first, obtaining the sub-image which includes the OD from the fundus image based on the saliency map; second, generating the super-pixel from the sub-image with a simple linear iterative clustering (SLIC) algorithm; third, classifying the super-pixel into OD or non-OD based on the AdaBoost algorithm; fourth, fitting the detected OD region with a circle based on the active geometric shape model. The proposed method has been evaluated on the Digital Retinal Images for Optic Nerve Segmentation (DRIONS) database. Experimental results show that our algorithm is very competitive with the state-of-the-art method.

**Index Terms**—Fundus image; Optic Disk Detection; Super-pixel; Machine Learning; Active Geometric Model; Computer Vision

## I. INTRODUCTION

Optic disk (OD) detection plays an important role in the fundus image analysis and computer aided diagnosis for ocular diseases, which has attracted extensive attentions from clinicians and researchers as an early stage detection method for ocular diseases. In addition, OD detection is often a key step for the detection of other anatomical structures [1], [2]. For example, the OD location helps to avoid false positive in the detection of exudates associated with diabetic retinopathy, since both of them are bright regions in the fundus image [3]. Besides, the vessels, which are of direct importance in assessing vascular condition, radiate from the OD, so tracking algorithms for vessels may start from there [2]. Moreover, the relationship between the size of the OD and the optic cup has been widely utilized for glaucoma diagnosis [3].

Among all algorithms for OD detection, the ones based on image processing are most popular. In the [4], [5], [6], the template-based methods are used for OD detection. The main idea of the template-based methods is to detect the edge first and then match the edge by the geometric shape fitting

approach, such as Circle Hough Transform. In [8], [9], [2], the deformable models are used to detect the OD. The deformable models converges the contour into the edge of interest in the image under the effect of the external and internal forces. In the deformable model, the design of the external force is one key step. In [2], the authors modified the active contours and exploited specific features of the OD anatomy. In [10], [3], [11], the morphological algorithms were used, which basically applied the watershed transformation to detect the OD. In particular, the authors in [3] proposed a stochastic watershed based method to detect the OD, which gives the best performance to the best of our knowledge.

In this paper, a new algorithm for OD detection is proposed, which combines several steps of treatments towards the original fundus image. In the proposed method, the sub-image is obtained first, and then the super-pixels are generated with the simple linear iterative clustering (SLIC) algorithm; the super-pixels are classified into OD or Non-OD by an AdaBoost algorithm. After locating the detected OD region, a circle is used to fit the OD with the active geometric shape model. The experimental results shows an improved performance (Area Overlap of 0.8433) compared with that of no-OD-fitting (Area Overlap of 0.8065) or fitting by Circle Hough Transform [4], [5] (Area Overlap of 0.7948). A flowchart of the proposed method is given in Fig 1.1.

The rest of the paper is organized as follows. The proposed method is described in Section II. The experimental results are presented in Section III, followed by a discussion in Section IV. The conclusions are drawn in Section V.

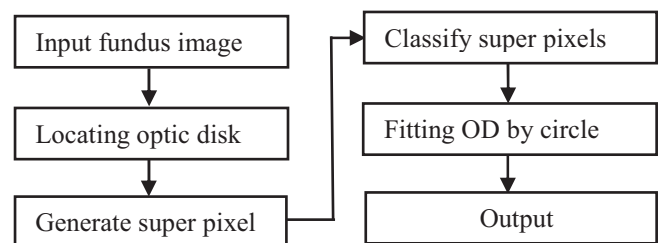


Fig.1.1 The flowchart of the proposed method

## II. METHODS

### A. OD Location

In order to obtain the sub-image from the fundus image, we need to locate the OD. Because the OD is more prominent in the fundus image, the saliency map is introduced. The saliency map is purported to represent the conspicuity—or “saliency”—at every location in the visual field by a scalar quantity and to guide the selection of attended locations, based on the spatial distribution of saliency [12]. Harel et. al [13] proposed a graph-based visual saliency. It is more reliable than the standard algorithm proposed by Itti et al [12].

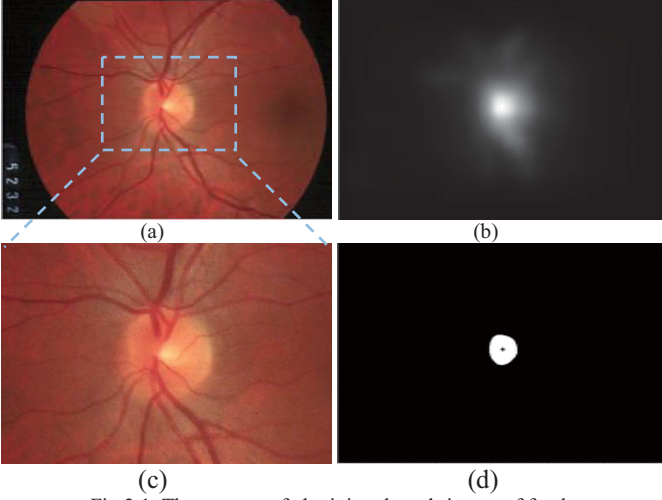


Fig.2.1. The process of obtaining the sub-image of fundus  
(a). The original image of fundus. (b). The saliency map of the original image.  
(c) The obtained sub-image, (d) The binary image of (b).

Taking advantage of the method proposed by Harel, we firstly convert the fundus image into a saliency map. Secondly, threshold processing is performed for the saliency map. Thirdly, we compute the centroid of the region obtained from the threshold processing. Finally, based on the centroid, the sub-image is obtained by cropping the fundus image. Fig.2.1 shows the experimental results as follows.

Fig. 2.1(a) gives an original fundus image; Fig. 2.1 (b) shows the saliency map of Fig. 2.1(a); Fig. 2.1(d) is the region after performing threshold processing on Fig. 2.1(b). It is worth to note that most of pixels in the region of Fig. 2.1(d) are located inside the OD. Finally, the centroid (black dot in Fig. 2.1(d)) of the region is used to crop the fundus image and obtain the sub-image, as shown in Fig. 2.1(c).

### B. Super-pixel Generation

Super-pixel algorithms group pixels into perceptually meaningful atomic regions which can be used to replace the rigid structure of the pixel grid [14]. It reduces the complexity of the image from thousands of pixels to only a few hundreds of super-pixels. Algorithms for generating super-pixel can be referred to in [14], [15], [16], [17]. In this paper, we use the SLIC [14] to generate the super-pixels in the fundus image since the SLIC has many advantages when compared with other super-pixel algorithms, such as simplicity, adhesion to boundaries and so on [14].

SLIC can be divided into three steps, namely, initialization, assignment and update.

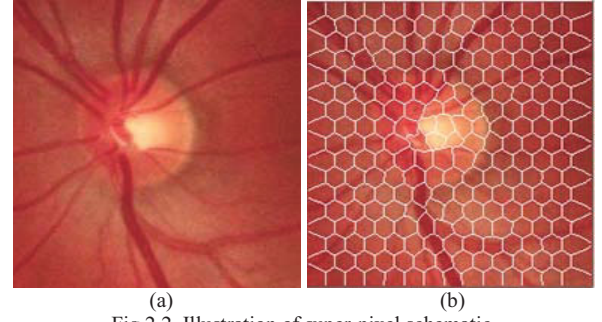


Fig.2.2. Illustration of super-pixel schematic.  
(a) The original sub-image. (b) Super-pixel of the original sub-image

First, in the initialization step,  $k$  cluster centers  $C_k$  are initialized by sampling pixels at regular grid with steps  $S$ , where  $S = \sqrt{N/K}$ ,  $N$  is the number of pixels and  $K$  is the number of the super-pixels. To avoid centering super-pixel on an edge and reduce the chance of seeding a super-pixel with a noisy pixel, centers are moved to the lowest gradient position in a  $3 \times 3$  neighborhood.

Second, in the assignment step, clustering is applied. For each pixel  $i$  in a  $2S \times 2S$  region around the center  $C_k$  the distance  $D$  between  $C_k$  and  $i$  is computed, then the pixel  $i$  is assigned to the nearest cluster center. The distance  $D$  is combined two parts. One is computed from the CIELAB color space  $[l, a, b]^T$ , and the other from the pixel’s position  $[x, y]^T$ . Doing so,  $D$  is written

$$D = \sqrt{\left(\frac{d_c}{N_c}\right)^2 + \left(\frac{d_s}{N_s}\right)^2} \quad (1)$$

Here,

$$d_c = \sqrt{(l_j - l_i)^2 + (a_j - a_i)^2 + (b_j - b_i)^2}$$

$$d_s = \sqrt{(x_j - x_i)^2 + (y_j - y_i)^2}$$

and  $N_c$ ,  $N_s$  are the normalization factor, namely their respective maximum distances within a cluster.

Third, in the update step, the new cluster centers based on the found pixel are computed. The iteration stops when the distance between the new center and the previous ones is small enough. Fig.2.2 shows the results of the super-pixel generation, where Fig. 2.2(a) is a sub-image, Fig. 2.2 (b) is the super-pixel schematic.

### C. Super-pixel Classification

For classifying the super-pixels as OD or non-OD, feature extraction is the first step. Ten features selected by the user are extracted in Table I.

After the step of feature extraction, the next step is feature selection. Since the Relief algorithm [21] does not depend on heuristics, is accurate even if features interact, and is noise-tolerant, so it is used to select the features in this work. The main idea of the Relief is assign a weight for each feature using statistical method [21].

After the feature extraction, the AdaBoost algorithm [18] is used to classify the super-pixels into OD or non-OD. The main

idea of the AdaBoost is to train a weak learner for each feature, and combine them as a strong learner. The pseudo-code of the AdaBoost is shown as Algorithm1 [18], [25].

TABLE I  
TEN FEATURES AS EXTRACTED BY THE USER

Features	Reasons of selection (Purposes)
Centroid of the super-pixel	It contains the location information of the super-pixel
The maximum and the minimum intensity value of the super-pixels in the red channel $I_r$ and the green channel $I_g$	The OD region basically shows as a bright region, which means that the intensity values of its pixels are mostly very large. On the other hand, the vessels also radiate from the OD region, which entails that there are also some pixels with very small intensity values in this region.
The mean and variance of the super-pixels in the red channel $I_r$ and the green channel $I_g$	To distinguish the super-pixels which are disturbed by noises from those undisturbed by noises.
The distances of the super-pixel centroid to the brightest super-pixel centroid	To distinguish the super-pixels consisting of the vessels which belong to the OD from those with vessels not belonging to the OD.

---

**Algorithm1. The pseudo-code of the AdaBoost**

---

**Input:** A set of hypothesis:  $h_1(x), \dots, h_T(x)$

A training set:  $(x_1, y_1), \dots, (x_m, y_m)$ ,  $x_i \in \mathcal{X}^n, y_i \in \{-1, 1\}$

**Output:** The final hypothesis:  $H(x) = \text{sign}(\sum_{i=1}^T \alpha_i h_i(x))$

Initialize the weighting coefficients  $D_1(i) = 1/m$

**for**  $t=1$  to  $T$  **do**

- a.** For each feature, train a weak classifier  $h_t(x)$  by minimizing the weighted error loss function

$$\varepsilon_t = \sum_{n=1}^N \omega_n^{(t)} I(h_t(x_n) \neq y_n)$$

- b.** Select the classifier  $h_t^*(x)$  with the lowest error  $\varepsilon_t^*$

- c.** Update the weighting coefficients as follows:

$$\alpha_t = \frac{1}{2} \ln \frac{1 - \varepsilon_t^*}{\varepsilon_t^*}$$

$$D_{t+1}(i) = \frac{D_t(i) \exp\{-\alpha_t y_i h_t^*(x_i)\}}{Z_t}$$

where  $Z_t$  is a normalization factor.

- d.** Output the final model:

$$H(x) = \text{sign}\left(\sum_{i=1}^T \alpha_i h_i^*(x)\right)$$

**end**

---

#### D. Fitting OD

After the classification, the boundary of the OD region is rough, as shown in Fig.2.3 (a). Based on the fact that the OD approximates a circle, in this work, a simple circle is used to fit the OD-contour, similar to [5]. However, we use an active geometric shape model [19] instead of the classical Circle

Hough Transform [5]. The detailed method is explained as follows.

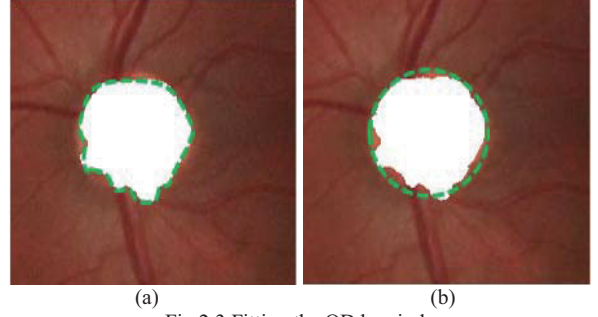


Fig.2.3 Fitting the OD by circle  
(a) A rough contour of the obtained region. (b) OD contour fitted by a circle

In the active contour model [20], the external and internal force fields need to be defined. The function of the external force is to push or pull the contour towards the boundary of interest. The external energy can be defined as [19]

$$E_{ext}^{(1)} = -\|\nabla I(x, y)\|^2 \quad (2)$$

$$E_{ext}^{(2)}(x, y) = -\|\nabla(G_\sigma(x, y) * I(x, y))\|^2 \quad (3)$$

where  $\nabla$  is the gradient operator,  $I(x, y)$  is a grayscale image. In (3),  $G_\sigma(x, y)$  is the Gaussian function which used to reduce the noise in the image and increase the capture range of the force field with standard deviation  $\sigma$ . If the image is a binary image, the external energy can be defined as

$$E_{ext}^{(3)} = I(x, y) \quad (4)$$

$$E_{ext}^{(4)} = G_\sigma(x, y) * I(x, y) \quad (5)$$

To enlarge the capture range, Xu [24] proposed a gradient vector field defined as  $\mathbf{v}(x, y) = [u(x, y), v(x, y)]$  that minimize the energy functional

$$\varepsilon = \iint \mu(u_x^2 + u_y^2 + v_x^2 + v_y^2) + \|\nabla f\|^2 \|\mathbf{v} - \nabla f\|^2 dx dy \quad (6)$$

where  $\mu$  is a regularization parameter governing the tradeoff between the first term and second term in integrand.  $f(x, y)$  is the negative of the external energy derived from the image  $I(x, y)$ , defined as

$$f(x, y) = -E_{ext}^{(i)}(x, y) \quad (7)$$

where  $i=1, 2, 3, 4$ . In this work, we use the gradient vector  $\mathbf{v}(x, y)$  and  $f(x, y) = -E_{ext}^{(4)}(x, y)$  since we operate on a binary image when fitting the OD by a circle.

The internal force is to maintain the shape of the contour. Since a circle is determined when the center and the radius are given, Wang et al [19] defined four internal forces to update the center, shown as below:

$$F_{ch} = \frac{1}{N} \sum_{i=1}^N \vec{F}(x_i, y_i) [1, 0]^T \quad (8)$$

$$F_{cv} = \frac{1}{N} \sum_{i=1}^N \vec{F}(x_i, y_i) [0, 1]^T \quad (9)$$

$$F_{cd} = \frac{1}{N} \sum_{i=1}^N \vec{F}(x_i, y_i) \left[ \frac{1}{\sqrt{2}}, \frac{1}{\sqrt{2}} \right]^T \quad (10)$$

$$F_{ca} = \frac{1}{N} \sum_{i=1}^N \vec{F}(x_i, y_i) \left[ -\frac{1}{\sqrt{2}}, \frac{1}{\sqrt{2}} \right]^T \quad (11)$$

Where

$$\vec{F}(x_i, y_i) = (F_x(x_i, y_i), F_y(x_i, y_i))$$

denotes the gradient at  $(x_i, y_i)$ ;  $F_{ch}$ ,  $F_{cv}$ ,  $F_{cd}$ ,  $F_{ca}$  are the horizontal, vertical, diagonal and anti-diagonal movement respectively. To update the radius, the average of the normal force is defined as [19]:

$$F_n = \frac{1}{N} \sum_{i=1}^N \vec{F}(x_i, y_i) \begin{bmatrix} \cos \theta_i \\ \sin \theta_i \end{bmatrix} \quad (12)$$

where  $\theta_i$  is the parameter corresponding to the  $(x_i, y_i)$ . The result after fitting the OD contour by the circle is shown in Fig.2.3 (b).

### III. EXPERIMENTAL RESULTS

Our proposed approach has been validated in the public dataset DRIONS [22], which contains 110 fundus images of 600×400 pixels with their ODs manually segmented by two different specialists. Similar to [3], the first expert's marks have been taken as the ground truth, to facilitate a comparison study with [3]. The mean age of the patients is 53.0 years, with 46.2% male and 53.8% female; all of them have the Caucasian ethnicity. 23.1% patients have chronic simple glaucoma and 76.9% of them have the eye hypertension. The images were acquired with a color analogical fundus camera. Some of the 110 images contain visual characteristics related to potential problems that may distort the detection process of OD-contour: artefacts (3 images), rim blurred or missing (5 images), moderate peripapillary atrophy (16 images), concentric peripapillary artefacts (20 images), and strong pallor distractor (6 images).

#### A. OD Detection Accuracy

In this work, the saliency map is used to locate the OD. The performance is carried out on the DRIONS database using 110 fundus images. OD detection is defined as “correct” if the detected OD center lies within the OD boundary [1]. By such definition, the OD detection accuracy of our approach achieves 99%, with only one image not correctly detected.

#### B. Classification Accuracy

As mentioned in Section II, the feature selection is performed before classification. The weight of each feature is obtained by Relief algorithm and the results are shown in Table II. From Table II, we can see that the variance intensity in  $I_r$  owns the greatest contribution (weight value of 0.0261) to the classification, and the maximum intensity in  $I_r$  has the least contribution (weight value of 0.0054).

After feature selection, classification is carried out by AdaBoost algorithm. In this work, if 60% components of the super-pixels are located in the OD, the OD is labeled as ‘1’, otherwise as ‘0’. The super-pixel classification is the 0-1

classification (OD or Non-OD). Thus, the classification accuracy is based on 0/1 loss [23], and the Ten-fold cross validation is used [23].

Table III shows the classification accuracy with different number of features. In Table III, the “Top 3” means the maximum weight of the first three features based on the Table II are used for classification, and so on. It can be observed that, the classification accuracy is improved with the increase of the number of the features. In this work, all of the features listed in Table II are used for the super-pixel classification.

TABLE II  
THE WEIGHT OF EACH FEATURE

Features	Weight
Centroid(x)	0.0177
Centroid(y)	0.0164
Mean Intensity in $I_g$	0.0070
Mean Intensity in $I_r$	0.0103
Max Intensity in $I_g$	0.0135
Max Intensity in $I_r$	0.0054
Min Intensity in $I_g$	0.0080
Min Intensity in $I_r$	0.0108
Distance	0.0105
Var Intensity in $I_g$	0.0116
Var Intensity in $I_r$	0.0261

TABLE III  
THE RELATIONSHIP BETWEEN THE FEATURES AND THE ACCURACY

Features	Accuracy
Top 3	0.9657
Top 6	0.9698
All	0.9739

In addition, the AdaBoost algorithm is compared with the SVM [23] and KNN [23]. The classification accuracy of all the compared algorithms are presented in Table IV. It is clear to see that AdaBoost algorithm obtains the best classification accuracy.

TABLE IV  
CLASSIFICATION ACCURACY OF DIFFERENT CLASSIFIERS

Methods	Accuracy
AdaBoost	0.9739
SVM	0.9680
KNN	0.9687

#### C. OD Segmentation

To measure the performance of the proposed method in the OD segmentation, the Area Overlap (AOL) is used. It is demonstrated in the Fig.3.1. We use the FN denotes false

negative, TP denotes true positive and FP false positive, then the Area Overlap [11] is defined as:

$$AOL = TP / (TP + FP + FN) \quad (13)$$

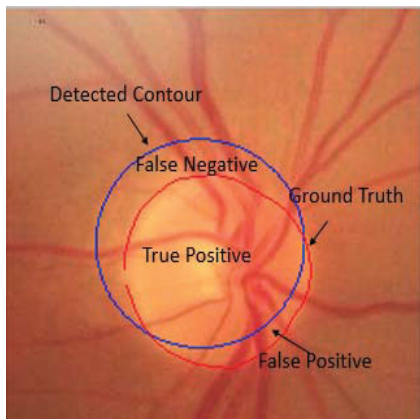


Fig.3.1 Areas used to find the overlap measure

The sensitivity analysis of the number of the super-pixel ( $K$ ) is also conducted, as shown in Fig.3.2. When  $K$  is equal to 250, the maximum value of the Area Overlap (0.8433) is achieved.

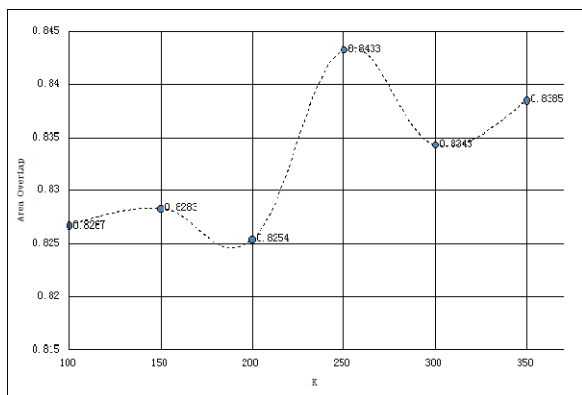


Fig.3.2. The relationship of  $k$  and Area Overlap

We also compare our approach with the state-of-the-art method in [3], as shown in Table V. It can be seen that the proposed method achieves very competitive results with the state-of-the-art method in the DRIONS database.

TABLE V  
COMPARISON OF THE AREA OVERLAP BY THE PROPOSED METHOD, BY THE S.MORALES PROPOSED METHOD

	Area Overlap
proposed	0.8433
S.Morales et al [3]	0.8423

#### D. Effectiveness of Active Geometric Model

The effect of active geometric model is evaluated in this section, compared with the classical method Circle Hough Transform [5] and the one without OD fitting process. Table VI shows the experimental results. It can be observed that the performance is the best (Area Overlap of 0.8433), when the geometric model is used to fit the OD.

TABLE VI  
ACTIVE GEOMETRIC MODEL VS CIRCLE HOUGH TRANSFORM

	Area Overlap
NO OD Fitting	0.8065
Circle Hough Trans.	0.7948
Geometric Model	0.8433

#### IV. DISCUSSION

In this paper, a new algorithm to detect the OD is proposed based on the machine learning and geometric model. First, the super-pixels of the sub-image are generated by SLIC algorithm. Then the AdaBoost algorithm is used to determine whether each super-pixel belong to the OD or not. This is a key step as high misclassification rate may cause bad performance in the subsequent OD fitting process. Fig. 4.1 shows such situation, where Fig. 4.1(a) denotes that too many super-pixels are misclassified, and in Fig. 4.2(b), it is notable that there is a large deviation between the detected OD contour (blue line) and the ground true (red line).

Even though higher classification accuracy is appreciated, the proposed method can tolerate the misclassification to some degree, especially when the misclassified super-pixels are not connected to the OD region, as shown in Fig. 4.2(a). In this case, to eliminate the impact of the misclassification, the largest connected region needs to be chosen before OD fitting. The Fig. 4.2 (b) shows that our method can tolerate the misclassification to some degree.

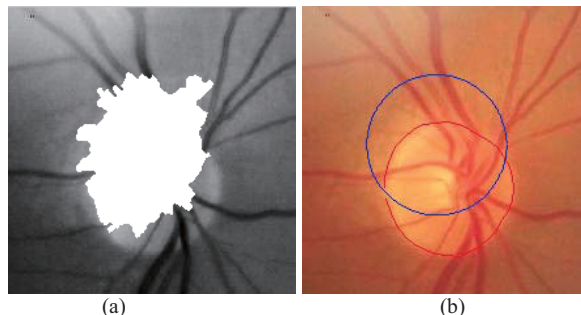


Fig. 4.1. The sketch map of high misclassification  
(a) Too many super-pixels are misclassified. (b) Unsatisfactory result

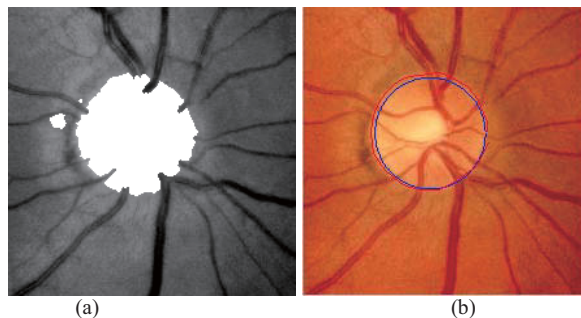


Fig. 4.2. the sketch map of the misclassification in a acceptable range  
(a) Misclassified super-pixels exist but can be tolerated by the algorithm.  
(b) Satisfactory result.

## V. CONCLUSION

In this paper, we proposed a new method for OD detection based on the machine learning and active geometric shape model. First, a sub-image is obtained by saliency map and then the super-pixel is generated using the SLIC algorithm. We select ten features to classify the super-pixel as OD or Non-OD with the AdaBoost algorithm and obtain the classification accuracy of 0.9739. Finally, we fit the OD by a circle using the active geometric shape model and the experimental result (Area Overlap of 0.8433) shows that the proposed method is very competitive with the state-of-the-art method [3].

## VI. ACKNOWLEDGEMENT

This work was supported in part by the National Natural Science Foundation of China (NSFC) under grant 61300159, 61175073 and 51375287, by the Natural Science Foundation of Jiangsu Province under grant BK20130808, by the Computer Numerical Control Machinery Product Innovation Special Foundation of Guangdong Province under grant 2013B011301015.

## REFERENCES

- [1] Shijian Lu, "Accurate and efficient optic disk detection and segmentation be a circular transformation," *IEEE Trans. Med. Imag.*, VOL.30, NO.12, 2011.
- [2] J. Lowell, A. Hunter, D. Steel, A. Basu, R.Ryder. 'Optic Nerve Head Segmentation,' *IEEE Trans. Med. Imag.*, VOL.23, 2004
- [3] S. Morales, V. Naranjo, J. Angulo, and M.Alcaniz, "Automatic detection optic disc based on PCA and mathematical morphology." *IEEE Trans. Med. Imag.*, VOL.32, NO.4, APRIL 2013.
- [4] M. Park, J. S. Jin, and S. Luo, "Locating the optic disc in retinal images," in *Proc. IEEE Int. Conf. Comput. Graph. Imag. Visualisat.*, 2006
- [5] A. Aquino, M. E. Gegundez-Arias, and D.Matin, "Detecting the optic disc boundary in digital fundus images using morphological, edge detection, and feature extraction techniques," *IEEE Trans. Med. Imag.*, 2010
- [6] M. Lalonde, M. Beaulieu, and L. Gagnon, "Fast and robust optic disc detection using pyramidal decomposition and Hausdorff-based template matching," *IEEE Trans. Med. Imag.*, 2001
- [7] T. Kauppi, and H. Kalviainen, "Simple and robust optic disc localization using colour decorrelated templates," in *Proc. 10<sup>th</sup> Int. Conf. Advanced Concepts for Intell. Vision Syst.*, 2008
- [8] A. Osareh, M. Mirmehdi, B. Thomas, and R.Markham, "Comparison of colour spaces for optic disc localisation in retinal images," in *Proc. 16<sup>th</sup> Int. Conf. Pattern Recognit.*, 2002
- [9] H. Li, and O. Cutatape, "Automated feature extraction in color retinal images by a model based approach," *IEEE Trans. Biomed. Eng.*, 2004
- [10] T. Walter, J. C. Klein, P. Massin, and A.Erginary, "A contribution of image processing to the diagnosis of diabetic retinopathy-detection of exudates in color fundus images of the human retina," *IEEE Trans. Med. Imag.*, vol.21, no.10, pp.1236-1243, Oct 2002
- [11] D. Welfer, A. Hunter, D. Steel, A. Basu, R. Ryder, E. Fletcher, and L. Keenedy "Segmentation of the optic disk in color eye fundus images using an adaptive morphological approach," *Comput. Biol. Med.*, 2010
- [12] L. Itti, C. Koch, and E. Niebur, "A model of saliency-based visual attention for rapid scene analysis," *IEEE Trans. Patter Anal. Mach. Intell.*, 1998
- [13] J. Harel, C. Koch, P. Perona, "Graph-based visual saliency," *California institute of technology Pasadena, CA 91125*
- [14] R.Achanta, A.Shaji, K.Smith, A.Luchhi, P.Fua, and S.Susstrunk, "Slic superpixels compared to state-of-the-art superpixel methods," *IEEE Trans. Patter Anal. Mach. Intell.*, vol. 34, no. 11, pp.2274-2281, Nov. 2012
- [15] P. Felzenszwalb and D. Huttenlocher, "Efficient graph-based image segmentation," *Int'l J. Computer Vision*, vol. 59, no. 2, pp. 167-181, Sept. 2004.
- [16] A. Vedaldi and S. Soatto, "Quick shift and kernel methods for mode seeking," *Proc. European Conf. Computer Vision*, 2008.
- [17] O. Veksler, Y. Boykov, and P. Mehrani, "Superpixels and supervoxels energy optimization framework," *Proc. European Conf. Computer Vision*, 2010
- [18] R.E. Schapire and Y. Singer, "Improved boosting algorithms using confidence-rated predictions," *Machine Learning*, 37(3):27-336, December 1999.
- [19] Q. Wang, K.L. Boyer, "The active geometric shape model: A new robust deformable shape model and its applications," *Computer Vision and Image Understanding* 116 (2012) 1178-1194
- [20] M. Kass, A. Witkin, D. Terzopoulos, "Snake: active contour models," *International Journal of Computer Vision* 1 (1988) 321-331
- [21] Kenji Kira, Larry A.Rendell. "The feature selection problem: traditional methods and a new algorithm," *AAAI-92 Proceedings*. Copyright@1992, AAAI(www.aaai.org). All rights reserved.]
- [22] <http://www.ia.uned.es/~ejcarmona/DRIONS-DB.html>
- [23] S. Rogers, M. Girolami, "A first course in machine learning," CRC Press, Version Date: 2011908, International Standard Book Number: 978-1-4398-2414-6, pp. 29-32
- [24] Chenyang Xu, Jerry L. Prince, "Snakes, Shapes, and Gradient Vector Flow," *IEEE TRANSACTIONS ON IMAGE PROCESSING*, VOL. 7, NO. 3, MARCH 1998
- [25] Jinchao Liu, "Passive Visual Sensing in Automatic Arc Welding," Kgs. Lyngby 2011, MAN-PHD-2011